

3D Coulomb Balls: Experiment and Simulation

O Arp¹, D Block¹, M Bonitz², H Fehske³, V Golubnychiy², S Kosse³,
P Ludwig^{2,4}, A Melzer³, and A Piel¹

¹ Christian-Albrechts-Universität Kiel, Institut für Experimentelle und Angewandte Physik,
24098 Kiel, Germany

² Christian-Albrechts-Universität Kiel, Institut für Theoretische Physik und Astrophysik,
24098 Kiel, Germany

³ Universität Greifswald, Institut für Physik, 17487 Greifswald, Germany

⁴ Universität Rostock, Fachbereich Physik, 18051 Rostock, Germany

Abstract. Spherically symmetric three-dimensional charged particle clusters are analyzed experimentally and theoretically. Based on accurate molecular dynamics simulations ground state configurations and energies with clusters for $N \leq 160$ are presented which correct previous results of Hasse and Avilov [Phys. Rev. A **44**, 4506 (1991)]. A complete table is given in the appendix. Further, the lowest metastable states are analyzed.

1. Introduction

Over the last years the investigation of complex (dusty) macroscopic and mesoscopic plasmas occurring e.g. in astrophysical, laboratory and technical situations has become an important research field. The theoretical description of complex plasmas is extremely difficult due to their heterogeneous composition and the drastic differences in the relevant space and times scales, e.g. [1, 2]. With the help of confinement potentials it has become possible to trap, for long periods of time, plasmas of a single charge (non-neutral plasmas). By varying the confinement strength researchers have achieved liquid behavior and even Coulomb crystallization of ions [3] and dust particles [4, 5]. Such strong correlation phenomena are of exceptional current interest in many fields.

In general, the formation of extended, three dimensional dust clouds in rf-discharges is hampered by the dominance of the gravitational force on the dust particles. Only in a narrow sheath region above the electrode the electric field forces can compensate gravity. Hence, typical dust clouds are two dimensional (2D) structures trapped in the non-equilibrium conditions of the boundary sheath which cause the formation of vertical particle chains [6].

Besides electric field forces thermophoresis is capable to compensate gravitation. This has recently been demonstrated by Rothermel et al. [7], but instead of homogeneous 3D dust clouds the formation of dust free regions in the center of the discharge was observed. Similar observations of these so-called voids are made under microgravity conditions [8]. Although in both situations the electric field force on the particle is directed towards the plasma center, the outward directed ion flow is assumed to produce a friction force which exceeds the electric field forces in the center of the discharge and hence creates the void.

This contribution deals with the simulation and analysis of spherically 3D clusters which were recently first experimentally observed in dusty plasmas [9]. We compare simulation results

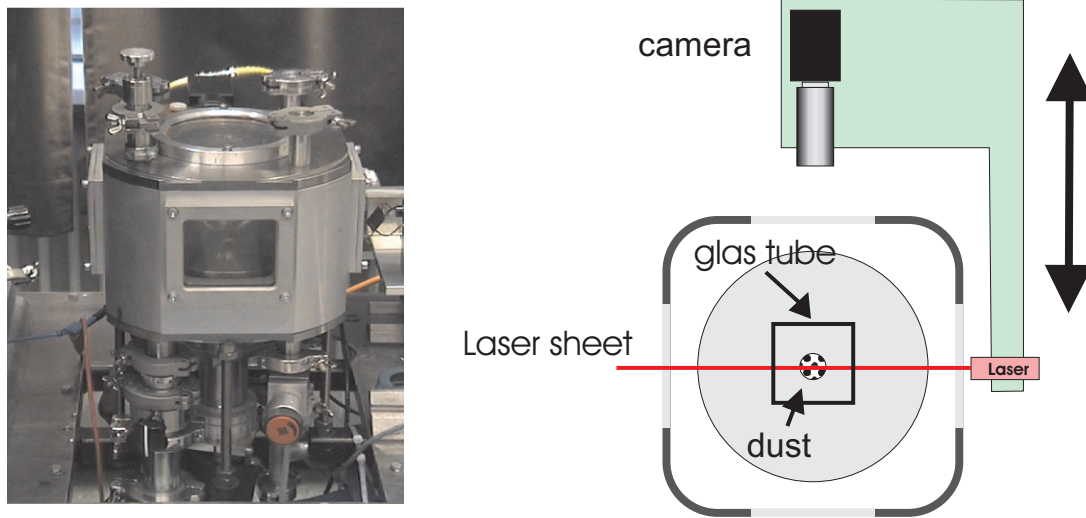


Figure 1. (Color online) Picture of the discharge chamber and a schematic drawing of the experimental setup (top view). The laser produces a vertical laser fan which illuminates vertical cross sections of the particle cloud. The camera looks at the illuminated plane under right angle. Laser and camera are mounted on a common positioning system to allow observation of arbitrary cross sections of the dust cloud.

to real dust clusters from experiments. In the simulations the dust-dust interaction potential is modelled by a Coulomb potential [10].

2. Experiments on Coulomb balls

2.1. Experimental Setup

The experiments presented in this paper are performed in a capacitively coupled rf-discharge in argon. The basic setup is well known from several investigations on 2D plasma crystals [6, 11–13]. It consists of two plane parallel electrodes. The rf-power is applied to the lower electrode with 17 cm diameter. The upper electrode is a mesh grid of similar size and is connected to ground. The distance between the electrodes is 6 cm. Compared to previous investigations two changes are applied to the setup. First, the temperature of the lower electrode can be controlled in a range between 20 – 80°C. With the upper electrode being at room temperature, vertical temperature gradients of up to 10°C/cm can be established. Second, a glass tube with square cross section is placed in the lower half of the discharge on top of the lower electrode.

Typical parameters for the discharge are vertical temperature gradients of 5 Kcm⁻¹, rf-power below 30 W and neutral gas pressures of 50-150 Pa. For the experiments we use particles with a diameter of 3.4 μm which are injected into the plasma from the top by gently shaking a fine sieve. The dust particles are illuminated by a vertical laser sheet of less than 500 μm width. The scattered light of the particles is observed with a CCD-camera under right angle (Fig. 1). The CCD camera is focused to the illuminated plane. Both, camera and laser fan are mounted on a common frame which can be moved in horizontal direction. Hence images of arbitrary cross section of the dust cloud can be recorded. In particular, all three coordinates of the particles can be determined from a systematic scan of the dust cloud.

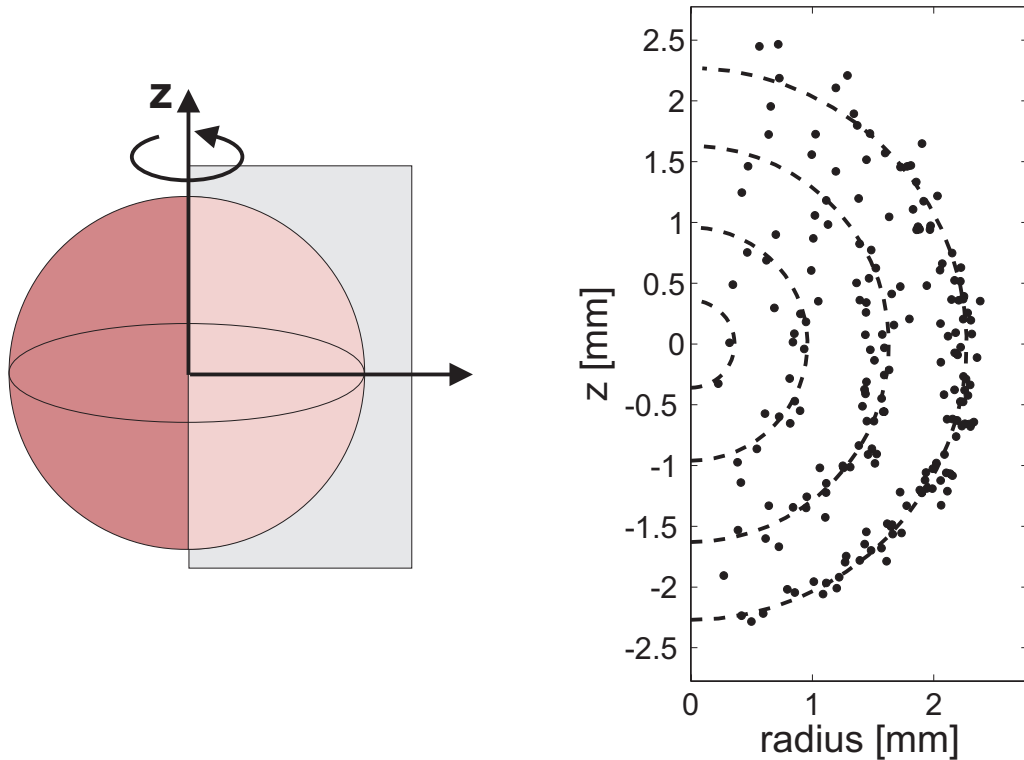


Figure 2. (Color online) The schematic drawing (left) shows a spherical particle cloud and a plane which rotates around an axis through the center of the cloud. The measured positions of all particles hitting this plane are marked with a dot for a particle cluster with 190 particles (right). The dashed lines indicate concentric circles around the cloud center.

2.2. Experimental Results

After injection of the particles the formation of a spherical dust cloud is observed. The cloud is located inside the glass tube close to the geometric center of the discharge arrangement. The example shown in Fig. 2 is a dust cloud consisting of 190 particles which has a diameter about 5 mm. In contrast to previous investigations [6–8] an important finding is that the dust cloud is void-free and that the particles show no chain formation. To investigate the spatial structure in more detail, Fig. 2 shows the particle distribution as a function of the cylindrical coordinates ρ and z , i.e. the azimuthal dependence is omitted in this plot. Besides the overall spherical shape of the dust cloud the occurrence of concentric shells is observed (dashed lines). This becomes evident when the particle position is plotted as a function of radius (spherical coordinates) only. Fig. 3 shows that the radial particle distribution function is strongly modulated. The prominent peaks indicate the formation of concentric spherical shells. A more detailed analysis [9] of the particle arrangement on individual shells shows that the particles arrange in a close hexagonal packing which includes few pentagonal defects to form a convex surface. The shell occupation for the 190 particle cluster is 2, 21, 60 and 107 starting with the innermost shell. This is close to the occupation number [10] found by numerical simulations of Coulomb clusters [20].

The appearance of a highly ordered particle system is further supported by calculations of the pair correlation function which yields a typical interparticle distance of 0.715 mm. Compared with the intershell distance of about 0.63 mm a good agreement with hexagonal closed packed systems is found [18].

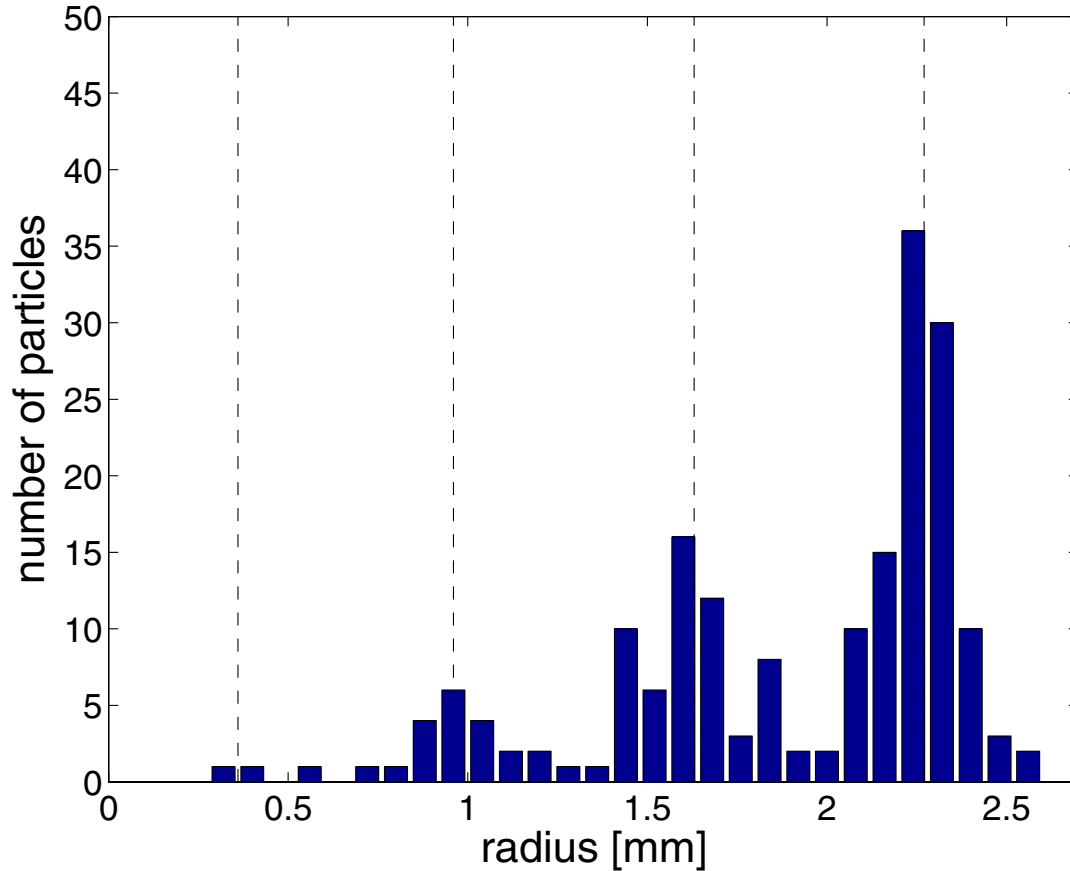


Figure 3. (Color online) Experimental radial particle distribution of a particle cluster with 190 particles.

3. Theory

3.1. Model

To model 3D Coulomb clusters confined in a 3D isotropic harmonic trap we consider N classical particles with equal charge q and mass m interacting via the Coulomb potential. The corresponding Hamilton function is

$$H_N = \sum_{i=1}^N \frac{m}{2} \dot{r}_i^2 + \sum_{i=1}^N \frac{m}{2} \omega^2 r_i^2 + \sum_{i>j}^N \frac{q^2}{4\pi\epsilon|\mathbf{r}_i - \mathbf{r}_j|}, \quad (1)$$

where ω is the strength of the confinement potential. In what follows below we will use dimensionless lengths and energies by introducing $r_0 = (q^2/2\pi\epsilon m\omega^2)^{1/3}$ and $E_0 = (m\omega^2 q^4/32\pi^2\epsilon^2)^{1/3}$. The length r_0 is the stable distance of two particles confined in the considered potential, E_0 denotes their ground state energy.

3.2. MD-Simulation

Three-dimensional classical Coulomb clusters in a spherical parabolic trap have been investigated earlier by different authors with different numerical methods. Rafac et al. [15] simulated the clusters with $N \leq 27$ using MC techniques. An extended table with $N \leq 59$ was given by Tsuruta et al. [16]. The work of Hasse et al. [18] the number of charged particles was increased up to a few

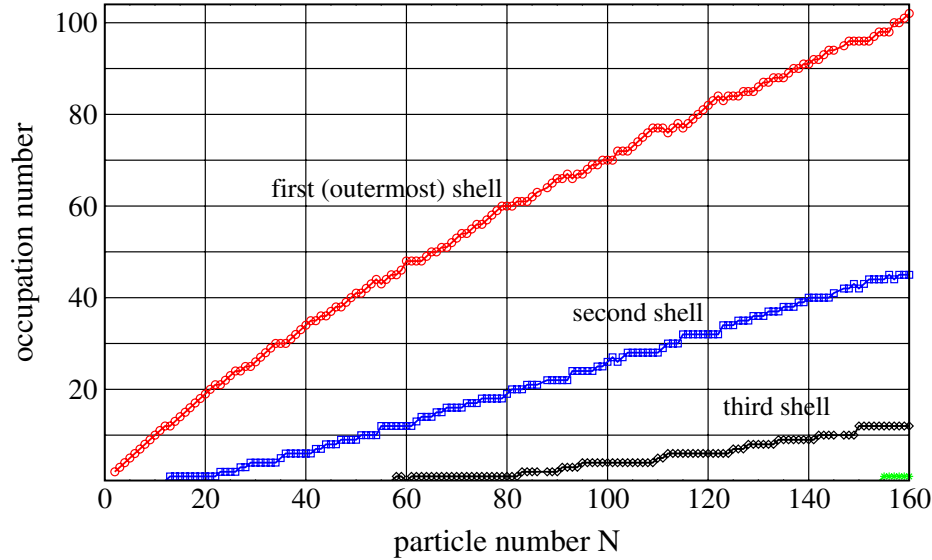


Figure 4. (Color online) Number of particles N_s on shell s vs. N . The 2nd shell is opened at $N = 13$, the 3rd shell at $N = 58$ (and $N = 61$), the 4th shell at $N = 155$. Note the reoccurrence of two shells at $N = 60$.

thousand. But they did not find the true ground state configurations for $N = 28 - 31, 44, 45$ and for clusters with more than 63 particles, due to accuracy limited calculation. To find the ground and metastable states, we used classical molecular dynamics (MD) together with a suitable *simulated annealing* method [10]. Starting with a random initial configuration of N particles, the system is cooled continuously until all momenta are zero and the particles settle in the minima of the potential energy surface. Depending on the particle number, the cooling down process was repeated up to several thousand times until every of the computed low energy states was found more than a given number of times (typically $10 \dots 100$) assuring a high probability that also the ground state has been found. Crucial for a high search efficiency is the use of an optimized MD time step (it has to be chosen not too small to avoid trapping in local potential minima). The complete results for $N = 2 \dots 160$ are given in Table 1 in the Appendix.

3.3. Cluster characterization

At zero temperature (zero particle velocities \dot{r}_i) concentric shells are found with characteristic closures as well as *magic* clusters. The stability of clusters is characterized by the *binding energy* [16]:

$$\Delta_2(N) = E(N + 1) + E(N - 1) - 2E(N). \quad (2)$$

The symmetry within the shells can be analyzed by performing a Voronoi analysis [10], i.e. by constructing polygons around each particle formed by the lines equally bisecting nearest-neighbor pairs on the shell. To quantify this topological criterion, we introduce the *Voronoi symmetry parameter* defined as

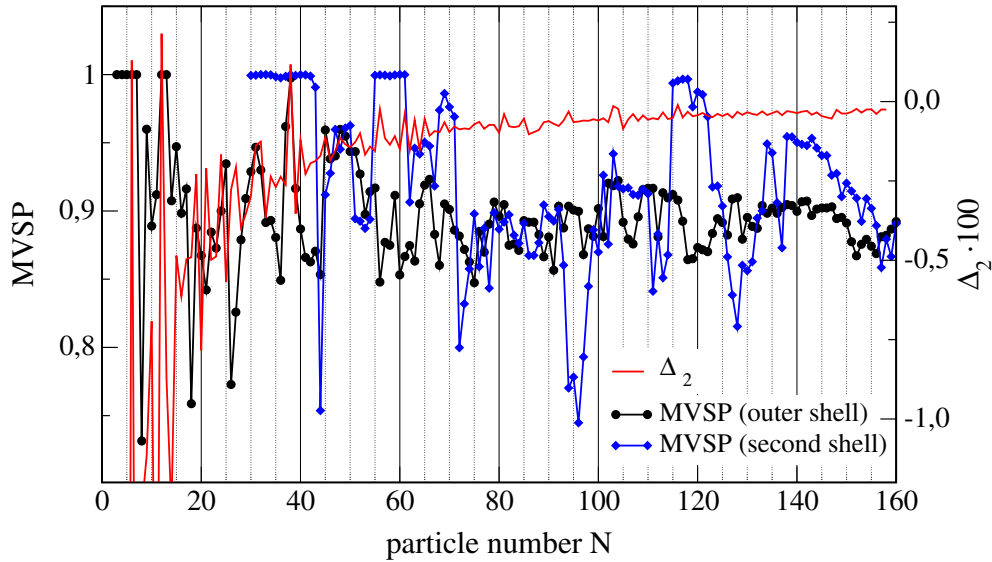


Figure 5. (Color online) Binding energy Δ_2 (Eq. 2) and mean Voronoi symmetry parameter MVSP (Eq. 4) of the two outermost shells vs. particle number N . Magic clusters are $N = 4, 6, 10, 12, 19, 32, 38, 56$ [16] and $N = 81, 94, 103, 116$ [10].

$$G_M = \frac{1}{N_M} \sum_{j=1}^{N_M} \frac{1}{M} \left| \sum_{k=1}^M e^{iM\theta_{jk}} \right|. \quad (3)$$

Here N_M denotes the number of particles on the shell, each of which is surrounded by a Voronoi polygon of order M (M nearest neighbors), and θ_{jk} is the angle between the j -th particle and its k -th nearest neighbor. A value $G_5 = 1$ ($G_6 = 1$) means that all pentagons (hexagons) are perfect, the reduction of G_M below 1 is a measure of their distortion. The Voronoi symmetry parameter G_M gives a measure for the symmetry of the Voronoi polygons of order M . To quantify the symmetry of the whole shell we introduce the *mean Voronoi symmetry parameter* (MVSP). We define the *mean Voronoi symmetry parameter* $\langle G^{(s)} \rangle$ of the s -th shell of the cluster as

$$\langle G^{(s)} \rangle = \frac{1}{N_s} \sum_M N_M G_M^{(s)}, \quad (4)$$

where N_s denotes the number of all particles on shell s . The MVSP allows to compare clusters with the same shell configuration because this parameter is very sensitive to the position of the particles within the cluster.

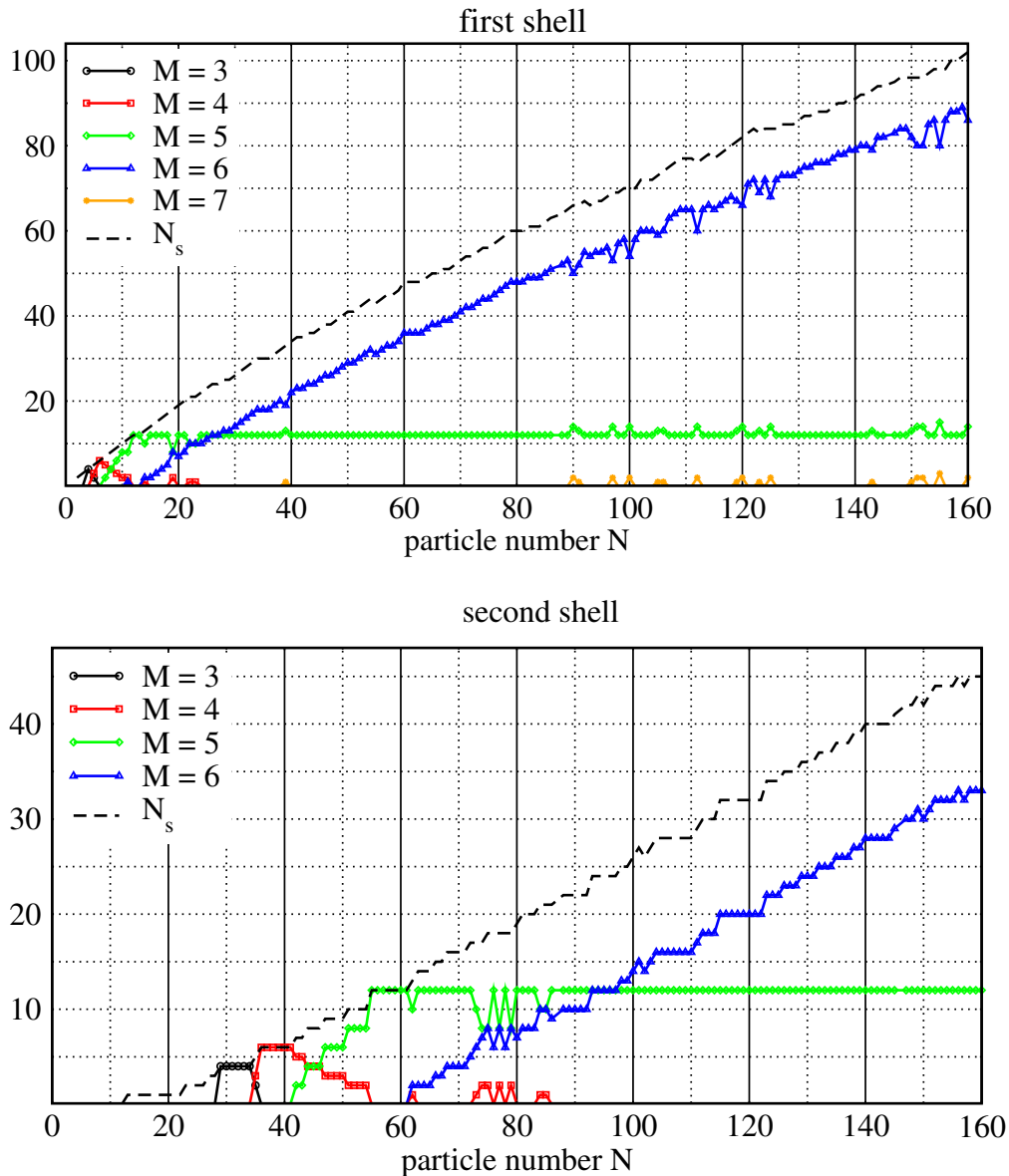


Figure 6. (Color online) Number N_M of Voronoi polygons with M edges in the two outermost shells vs. total particle number N . The top figure shows the first (outermost) shell and the bottom figure the second shell.

3.4. Analysis of 3D Coulomb Clusters

Figure 4 shows the number of particles on different shells of the Coulomb clusters as a function of the total particle number. The figure is easy to understand. For $N \leq 12$ all particles occupy one shell. With $N = 12$, the shell is filled completely (closed shell). The 13th particle opens a new shell, i.e. one particle from the outer shell goes inside. Analogously, the 2nd shell is closed when it contains 12 particles (for $N = 57$), and the 3rd shell is closed for $N = 154$, see table 1.

The existence of the shell structure is a marked peculiarity of mesoscopic Coulomb systems, and is, of course, caused by the spherical confinement potential. With increasing N the structure of a macroscopic system emerges gradually, see also Ref. [19]. The effect of the confinement is

strongest at the cluster boundary, i.e. in the outer shell, whereas the inner shells are partially shielded from the trap potential by the surrounding particle shells. Therefore, bulk properties start to emerge in the center. This trend is, in fact, clearly seen already for $N \leq 200$ by comparing the widths of the shells [10], see table 1.

For the clusters ($N = 2 \dots 160$) Fig. 5 shows the binding energy Δ_2 (Eq. 2) of the clusters and the MVSP (Eq. 4) of the two outermost shells vs. the particle number. With the help of these two quantities one can identify the so-called *magic clusters*, which are particularly stable. The combination of these quantities (a peak in Δ_2 and a higher MVSP in the shells) allows us to identify magic clusters: $N = 4, 6, 10, 12, 19, 32, 38, 56$ [16] and $N = 81, 94, 103, 116$ [10].

Now we analyze the symmetry of the clusters in more detail. Figure 6 shows the number of Voronoi polygons with M edges on the two outermost shells vs. total particle number. The dashed line in the figures gives the number of particles on the shell. With increasing size the particle number in the shell is increasing too. For smaller particle numbers in the shell we observe polygons with $M = 3, 4$. With increasing particle numbers one can see an increase of the number of polygons with $M = 6$, the number of polygons with $M = 5$ grows up to 12 and is then nearly constant. In each case Euler's theorem $\sum_{M(M \geq 3)} (6 - M)N_M = 12$ is fulfilled.

3.5. Cluster Fine Structure

An interesting observation is that the simulations frequently yield for the same shell configuration different values of the total energy, see e.g. [10]. The differences are much larger than the simulation error, moreover, the energies are reproducible. Obviously the state of a cluster is not completely determined by its shell configuration (contrary to the 2D case). There exist further (excited) states, which have the same shell configuration as the ground state, but a *different particle arrangement and symmetry within one shell*. This can be called *fine structure*. To understand the differences in the structure of these states with same shell configuration we analyze the intrashell symmetry by a Voronoi analysis, i.e. by constructing polygons around a given particle formed by the planes equally bisecting nearest-neighbor pairs on the shell (cf. the example of $N = 17$ shown in Fig. 7). Interestingly, both states do not differ with respect to the number of polygons of each kind in the outer shell: there are $N_5 = 12$ pentagons and $N_6 = 4$ hexagons. Rather the *arrangement of the polygons* is different. In one case, the four hexagons form a perfect tetrahedron ABCD and are separated from each other by pentagons, cf. Fig. 7 (left), in the other case two pairs of hexagons touch, see Fig. 7 (right) and the tetrahedron is distorted (Fig. 8). Two edges remain practically constant ($\overline{AB} \approx \overline{CD} \approx 1.63$), but the edge \overline{AB} rotates with respect to the first case by an angle of 34 degrees resulting in a reduction of edges \overline{BC} and \overline{AD} to about 1.24 while \overline{AC} and \overline{BD} increase to 1.94. Comparing the energies of the two configurations we conclude that the state with the more symmetric arrangement of the Voronoi polygons, i.e. (Fig. 7, left), has the lower energy.

4. Summary and Outlook

In this contribution we have presented numerical simulation results for spherical Coulomb clusters with $N \leq 160$. The observed lowest energy states for $N \geq 60$ are, in most cases, lower than those previously reported and should be reliable baring points for experiments with classical Coulomb balls in dusty plasmas or ultracold ions. Moreover, the shell configurations detected are expected to be important also for quantum Coulomb clusters (e.g. in quantum dots) in the strong coupling limit, as for 2D systems it was found that in most cases they have the same shell configuration as their classical counterpart [14, 17]. In addition we performed an analysis of the lowest excited states of small clusters. Besides metastable states with a shell structure different from the ground state we identified *fine structure* states which are characterized by different particle arrangement within the shells. These states have a lower symmetry which is

Ground state (16,1)

$$\begin{aligned}
 E/N &= 6.388610 \\
 r_1 &= 1.5042 \\
 G_5 &= 0.891 \quad [12] \\
 G_6 &= 0.993 \quad [4] \\
 \langle G^{(1)} \rangle &= 0.916
 \end{aligned}$$

First meta-stable state (16,1)

$$\begin{aligned}
 E/N &= 6.388975 \\
 r_1 &= 1.5042 \\
 G_5 &= 0.746 \quad [12] \\
 G_6 &= 0.884 \quad [4] \\
 \langle G^{(1)} \rangle &= 0.781
 \end{aligned}$$

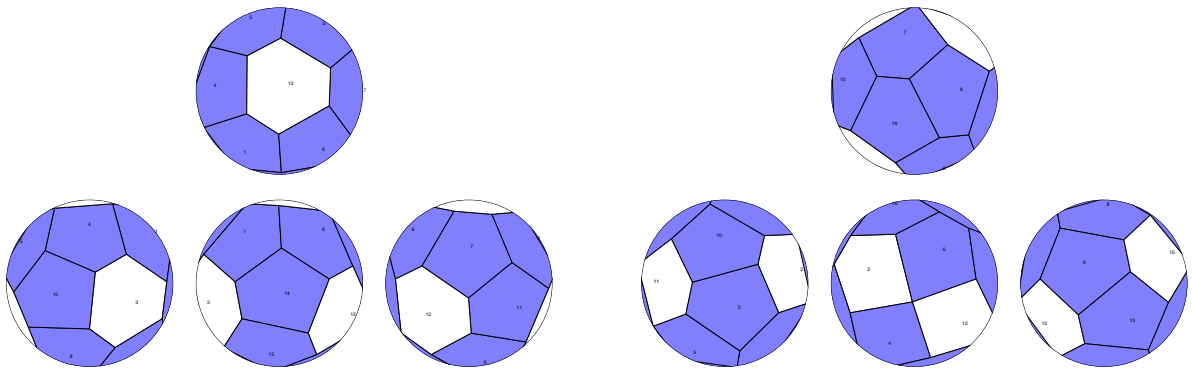


Figure 7. (Color online) Voronoi construction for the cluster $N = 17$. The two energetically lowest states with shell configuration $N = \{1, 16\}$ are shown. White (dark) areas are hexagons (pentagons) – indicating the number of nearest neighbors of the corresponding particle. Left: ground state, right: first excited (*fine structure*) state. Above the figures the energies, radius of the shell r_1 and the symmetry parameters are given.

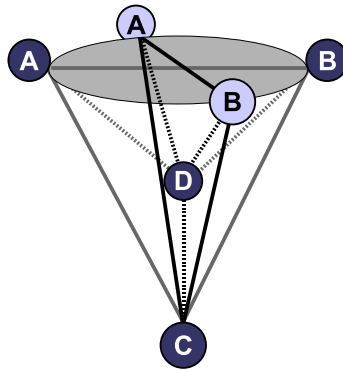


Figure 8. (Color online) Arrangement of the four particles surrounded by hexagons – the two states differ by rotation of the edge AB . Dark (bright) circles corresponds to the configuration shown in Fig. 7, left (right).

linked to higher values of the total energy. Despite the decreasing values of the excitation energy with increasing N , knowledge of the lowest metastable states is important for understanding the dynamic properties of mesoscopic clusters.

From the experimental point of view creation of spherical particle clouds consisting of a relatively large number of charged particles (of order 100 and higher) is rather easily achieved. Creation of small clusters with a predefined number of particles is still under implementation in the experiment. On the other hand, computer simulations become very time consuming for $N > 200$. First preliminary comparisons of experiments and theory show good qualitative agreement of the shell structure of the cluster $N = 190$. The agreement is further improved if a statically screened Coulomb potential (i.e. Yukawa potential) is used instead of the bare Coulomb interaction [20]. However, extensive further comparisons for various N are necessary.

References

- [1] Morfill G.E. and Kersten H 2003 *New J. Phys.* **5**
- [2] Dubin D H E and O'Neill T M 1999 *Rev. Mod. Phys.* **71** 87
- [3] Itano W M, Bollinger J J, Tan J N, Jelenkovic B and Wineland D J 1998 *Science* **297** 686
- [4] Thomas H, Morfill G E, Demmel V, Goree J, Feuerbacher B and Möhlmann D 1994 *Phys. Rev. Lett.* **73** 652
- [5] Hayashi Y and Tachibana K 1994 *Jpn. J. Appl. Phys.* **33** L804
- [6] Melzer A, Schweigert V and Piel A 2000 *Phys. Scripta* **61** 494
- [7] Rothermel H, Hagl T, Morfill G E, Thoma M H and Thomas H M 2002 *Phys. Rev. Lett.* **89** 175001
- [8] Morfill G E, Thomas H M, Konopka U, Rothermel H, Zuzic M, Ivlev A and Goree J 1999 *Phys. Rev. Lett.* **83** 1598
- [9] Arp O, Block D, Melzer A and Piel A 2004 *Phys. Rev. Lett.* **93** 165004
- [10] Ludwig P, Kosse S and Bonitz M 2005 *Phys. Rev. E* accepted (*Preprint* arXiv:physics/0409095)
- [11] Trottenberg T, Melzer A and Piel A 1995 *Plasma Sources Sci. Technol.* **4** 450
- [12] Homann A, Melzer A, Madani R and Piel A 1998 *Phys. Lett. A* **242** 173
- [13] Klindworth M, Melzer A, Piel A and Schweigert V 1999 *Phys. Rev. B.* **61** 3194
- [14] Ludwig P, Filinov A V, Bonitz M and Lozovik Yu E 2003 *Contrib. Plasma Phys.* **43** 285
- [15] Rafac R, Schiffer J P, Hangst J S, Dubin D H E and Wales D J 1991 *Proc. Natl. Acad. Sci. USA* **88** 483
- [16] Tsuruta K and Ichimaru S 1993 *Phys. Rev. A* **48** 1339
- [17] Filinov A V, Bonitz M and Lozovik Yu E 2001 *Phys. Rev. Lett.* **86** 3851
- [18] Hasse R W, Avilov V V 1991 *Phys. Rev. A* **44** 4506
- [19] Schiffer J P 2002 *Phys. Rev. Lett.* **88** 205003
- [20] Ludwig P, Golubnichiy V and Bonitz M, unpublished

Appendix

Table 1. Ground state shell configurations, energy per particle, mean shell radii $r_{1,2,3,4}$ and widths $\sigma_{1,2,3,4}$

N	Config.	E/N	r_1	r_2	σ_1	σ_2
2	(2)	0.5	0.500(0)	-	0.000(0)	-
3	(3)	1.310370(7)	0.660(9)	-	0.000(0)	-
4	(4)	1.785826(2)	0.771(5)	-	0.000(0)	-
5	(5)	2.245187(2)	0.865(1)	-	0.010(0)	-
6	(6)	2.654039(0)	0.940(6)	-	0.000(0)	-
7	(7)	3.064186(0)	1.010(6)	-	0.013(5)	-
8	(8)	3.443409(4)	1.071(4)	-	0.000(0)	-
9	(9)	3.809782(0)	1.126(9)	-	0.006(3)	-
10	(10)	4.164990(0)	1.178(3)	-	0.005(5)	-
11	(11)	4.513275(4)	1.226(5)	-	0.010(1)	-
12	(12)	4.838966(4)	1.270(0)	-	0.000(0)	-
13	(12, 1)	5.166798(3)	1.365(9)	-	0.000(0)	-
14	(13, 1)	5.485915(4)	1.403(3)	0.007(1)	0.005(8)	-
15	(14, 1)	5.792094(2)	1.438(3)	0.000(0)	0.005(6)	-
16	(15, 1)	6.093421(3)	1.471(9)	0.000(0)	0.005(2)	-
17	(16, 1)	6.388609(9)	1.504(2)	0.000(0)	0.006(2)	-
18	(17, 1)	6.678830(3)	1.535(3)	0.000(0)	0.000(6)	-
19	(18, 1)	6.964146(0)	1.565(4)	0.000(0)	0.004(0)	-
20	(19, 1)	7.247181(0)	1.594(6)	0.000(2)	0.006(9)	-
21	(20, 1)	7.522377(7)	1.622(6)	0.000(0)	0.003(4)	-
22	(21, 1)	7.795468(9)	1.649(9)	0.000(7)	0.006(3)	-
23	(21, 2)	8.063575(4)	1.707(7)	0.530(2)	0.030(2)	-
24	(22, 2)	8.326802(8)	1.732(6)	0.526(0)	0.029(4)	0.009(2)
25	(23, 2)	8.588360(7)	1.757(0)	0.526(2)	0.026(3)	0.000(0)
26	(24, 2)	8.844236(2)	1.780(5)	0.524(1)	0.026(3)	0.000(8)
27	(24, 3)	9.097334(6)	1.830(5)	0.689(8)	0.036(9)	0.009(6)
28	(25, 3)	9.348367(8)	1.852(5)	0.688(9)	0.036(4)	0.001(6)
29	(25, 4)	9.595435(1)	1.899(2)	0.798(7)	0.037(4)	0.011(9)
30	(26, 4)	9.838964(7)	1.919(7)	0.796(1)	0.034(7)	0.018(0)
31	(27, 4)	10.079511(0)	1.939(9)	0.792(6)	0.038(3)	0.007(1)
32	(28, 4)	10.318678(8)	1.959(6)	0.793(5)	0.033(8)	0.000(0)
33	(29, 4)	10.556587(1)	1.979(1)	0.791(4)	0.034(6)	0.010(7)
34	(30, 4)	10.790841(9)	1.998(0)	0.790(1)	0.035(8)	0.000(0)
35	(30, 5)	11.022731(0)	2.038(1)	0.885(9)	0.041(0)	0.038(0)
36	(30, 6)	11.251922(6)	2.077(5)	0.958(2)	0.035(3)	0.000(0)
37	(31, 6)	11.478747(2)	2.094(7)	0.958(5)	0.035(8)	0.017(8)
38	(32, 6)	11.702951(6)	2.111(9)	0.954(9)	0.039(4)	0.000(0)
39	(33, 6)	11.928322(8)	2.128(9)	0.954(9)	0.035(2)	0.012(0)
40	(34, 6)	12.150162(9)	2.145(3)	0.954(7)	0.038(0)	0.011(8)
41	(35, 6)	12.370791(5)	2.161(8)	0.953(8)	0.035(4)	0.006(4)
42	(35, 7)	12.589139(3)	2.196(1)	1.026(0)	0.040(6)	0.050(7)
43	(36, 7)	12.805545(2)	2.211(9)	1.025(2)	0.037(4)	0.045(6)
44	(36, 8)	13.020077(9)	2.245(4)	1.084(5)	0.038(0)	0.013(2)
45	(37, 8)	13.232901(2)	2.260(3)	1.084(5)	0.038(0)	0.034(0)

Continuation of Table 1

N	Config.	E/N	r_1	r_2	r_3	σ_1	σ_2	σ_3
46	(38, 8)	13.444601(5)	2.275(1)	1.084(2)	-	0.036(4)	0.037(3)	-
47	(38, 9)	13.654458(5)	2.306(6)	1.139(1)	-	0.034(0)	0.048(8)	-
48	(39, 9)	13.862762(0)	2.321(0)	1.137(9)	-	0.033(0)	0.036(2)	-
49	(40, 9)	14.069919(9)	2.335(1)	1.137(1)	-	0.034(1)	0.035(4)	-
50	(41, 9)	14.275728(5)	2.349(0)	1.137(2)	-	0.036(8)	0.026(7)	-
51	(41, 10)	14.480101(0)	2.378(8)	1.187(7)	-	0.035(2)	0.029(8)	-
52	(42, 10)	14.683192(6)	2.392(2)	1.187(5)	-	0.034(0)	0.029(4)	-
53	(43, 10)	14.885283(9)	2.405(5)	1.187(2)	-	0.037(5)	0.029(5)	-
54	(44, 10)	15.085702(8)	2.418(6)	1.187(2)	-	0.035(2)	0.024(5)	-
55	(43, 12)	15.284702(6)	2.461(8)	1.277(3)	-	0.031(8)	0.010(1)	-
56	(44, 12)	15.482144(4)	2.474(3)	1.278(0)	-	0.036(9)	0.010(1)	-
57	(45, 12)	15.679350(2)	2.486(9)	1.276(3)	-	0.036(3)	0.007(2)	-
58	(45, 12, 1)	15.875406(2)	2.512(6)	1.376(5)	0.005(2)	0.046(3)	0.004(3)	-
59	(46, 12, 1)	16.070103(4)	2.524(7)	1.376(4)	0.000(0)	0.048(0)	0.000(0)	-
60	(48, 12)	16.263707(3)	2.523(6)	1.275(5)	-	0.036(0)	0.003(6)	-
61	(48, 12, 1)	16.455812(8)	2.548(8)	1.375(1)	0.004(2)	0.045(1)	0.002(4)	-
62	(48, 13, 1)	16.647519(7)	2.573(8)	1.413(4)	0.016(3)	0.044(3)	0.023(5)	-
63	(48, 14, 1)	16.837694(0)	2.598(8)	1.447(3)	0.004(6)	0.039(3)	0.024(7)	-
64	(49, 14, 1)	17.027288(9)	2.610(1)	1.447(8)	0.001(9)	0.037(3)	0.023(7)	-
65	(50, 14, 1)	17.215360(8)	2.621(2)	1.447(7)	0.000(0)	0.049(5)	0.018(8)	-
66	(50, 15, 1)	17.402891(3)	2.645(3)	1.480(5)	0.005(9)	0.043(2)	0.026(6)	-
67	(51, 15, 1)	17.589347(4)	2.656(3)	1.480(3)	0.004(6)	0.043(0)	0.024(3)	-
68	(51, 16, 1)	17.774874(4)	2.679(7)	1.512(3)	0.003(4)	0.034(5)	0.031(1)	-
69	(52, 16, 1)	17.959432(2)	2.690(3)	1.512(6)	0.001(0)	0.039(3)	0.034(3)	-
70	(53, 16, 1)	18.143338(3)	2.701(0)	1.511(9)	0.002(3)	0.041(1)	0.031(7)	-
71	(54, 16, 1)	18.326281(9)	2.711(6)	1.511(8)	0.008(3)	0.041(2)	0.028(0)	-
72	(54, 17, 1)	18.508444(3)	2.734(2)	1.542(3)	0.005(9)	0.035(3)	0.020(1)	-
73	(55, 17, 1)	18.689729(4)	2.744(5)	1.542(2)	0.004(7)	0.037(5)	0.020(4)	-
74	(56, 17, 1)	18.870167(9)	2.754(6)	1.542(3)	0.008(8)	0.042(2)	0.017(8)	-
75	(56, 18, 1)	19.049742(1)	2.776(5)	1.571(7)	0.005(5)	0.037(2)	0.031(8)	-
76	(57, 18, 1)	19.228600(2)	2.786(5)	1.571(4)	0.000(0)	0.037(2)	0.025(3)	-
77	(58, 18, 1)	19.406816(5)	2.796(4)	1.571(4)	0.003(3)	0.038(5)	0.031(4)	-
78	(59, 18, 1)	19.584175(2)	2.806(3)	1.571(5)	0.004(6)	0.039(8)	0.027(1)	-
79	(60, 18, 1)	19.760799(9)	2.816(1)	1.570(9)	0.005(0)	0.040(2)	0.027(4)	-
80	(60, 19, 1)	19.936689(9)	2.837(0)	1.600(2)	0.003(0)	0.038(4)	0.038(4)	-
81	(60, 20, 1)	20.111592(4)	2.857(7)	1.627(1)	0.006(4)	0.031(1)	0.040(6)	-
82	(61, 20, 1)	20.286103(1)	2.867(1)	1.627(4)	0.005(0)	0.031(1)	0.040(6)	-
83	(61, 20, 2)	20.459834(2)	2.886(6)	1.688(6)	0.544(7)	0.039(0)	0.061(9)	0.044(5)
84	(61, 21, 2)	20.632758(9)	2.906(4)	1.714(0)	0.542(6)	0.034(1)	0.069(2)	0.003(3)
85	(62, 21, 2)	20.804907(5)	2.915(6)	1.713(5)	0.542(2)	0.038(6)	0.063(9)	0.021(7)
86	(63, 21, 2)	20.976517(8)	2.924(7)	1.713(8)	0.540(3)	0.041(2)	0.061(4)	0.009(6)
88	(64, 22, 2)	21.317682(0)	2.953(2)	1.737(8)	0.538(5)	0.033(9)	0.059(1)	0.005(7)
89	(65, 22, 2)	21.487369(1)	2.962(1)	1.737(8)	0.537(5)	0.034(4)	0.057(0)	-
90	(66, 22, 2)	21.656403(7)	2.970(9)	1.737(6)	0.535(9)	0.037(4)	0.057(5)	-

Continuation of Table 1

N	Config.	E/N	r_1	r_2	r_3	σ_1	σ_2	σ_3
91	(66, 22, 3)	21.824823(2)	2.989(1)	1.791(6)	0.705(0)	0.043(4)	0.066(7)	0.004(0)
92	(67, 22, 3)	21.992541(8)	2.997(9)	1.791(1)	0.705(2)	0.044(4)	0.064(9)	0.015(2)
93	(66, 24, 3)	22.159489(7)	3.026(0)	1.836(1)	0.701(9)	0.035(8)	0.078(1)	0.013(0)
94	(67, 24, 3)	22.325841(4)	3.034(7)	1.835(6)	0.700(1)	0.034(9)	0.068(3)	0.019(6)
95	(67, 24, 4)	22.491878(2)	3.052(2)	1.884(8)	0.808(9)	0.035(3)	0.067(7)	0.021(5)
96	(68, 24, 4)	22.657270(6)	3.060(6)	1.884(6)	0.808(3)	0.040(8)	0.067(5)	0.033(0)
97	(69, 24, 4)	22.822032(2)	3.068(7)	1.884(9)	0.809(5)	0.046(1)	0.067(8)	0.029(9)
98	(69, 25, 4)	22.986199(1)	3.086(4)	1.905(5)	0.808(1)	0.035(7)	0.075(0)	0.028(0)
99	(70, 25, 4)	23.149758(0)	3.094(5)	1.905(6)	0.807(1)	0.043(0)	0.072(2)	0.027(9)
100	(70, 26, 4)	23.312759(3)	3.111(7)	1.925(9)	0.805(5)	0.041(7)	0.074(0)	0.022(6)
101	(70, 27, 4)	23.475164(4)	3.129(1)	1.945(0)	0.802(8)	0.030(1)	0.073(1)	0.005(8)
102	(72, 26, 4)	23.637044(1)	3.128(0)	1.924(8)	0.805(2)	0.043(3)	0.071(0)	0.018(9)
103	(72, 27, 4)	23.798274(3)	3.145(1)	1.944(3)	0.801(7)	0.037(7)	0.071(2)	0.008(2)
104	(72, 28, 4)	23.959361(3)	3.161(7)	1.964(1)	0.802(1)	0.034(5)	0.078(1)	0.001(9)
105	(73, 28, 4)	24.120222(9)	3.169(6)	1.964(1)	0.802(0)	0.036(3)	0.076(8)	0.010(2)
106	(74, 28, 4)	24.280223(2)	3.177(3)	1.964(2)	0.802(3)	0.038(7)	0.077(2)	0.009(2)
107	(75, 28, 4)	24.439665(7)	3.185(0)	1.964(0)	0.801(0)	0.040(4)	0.074(4)	0.006(7)
108	(76, 28, 4)	24.598713(7)	3.192(7)	1.964(0)	0.800(7)	0.041(0)	0.072(3)	0.005(3)
109	(77, 28, 4)	24.757151(3)	3.200(5)	1.963(8)	0.800(6)	0.040(6)	0.070(5)	0.003(4)
110	(77, 28, 5)	24.915153(9)	3.216(3)	2.006(3)	0.896(1)	0.043(5)	0.076(3)	0.041(5)
111	(77, 29, 5)	25.072584(2)	3.232(2)	2.024(9)	0.896(9)	0.040(9)	0.081(7)	0.030(3)
112	(76, 30, 6)	25.229492(1)	3.255(4)	2.085(7)	0.967(0)	0.035(8)	0.095(0)	0.041(7)
113	(77, 30, 6)	25.385842(0)	3.263(7)	2.083(1)	0.964(0)	0.036(8)	0.073(2)	0.016(9)
114	(78, 30, 6)	25.541848(2)	3.271(1)	2.082(9)	0.964(0)	0.036(6)	0.074(5)	0.009(6)
115	(77, 32, 6)	25.697308(2)	3.294(9)	2.116(2)	0.963(0)	0.026(6)	0.077(4)	0.004(4)
116	(78, 32, 6)	25.852252(8)	3.302(2)	2.115(9)	0.963(3)	0.021(8)	0.076(0)	0.004(5)
117	(79, 32, 6)	26.007089(4)	3.309(4)	2.115(8)	0.962(2)	0.032(4)	0.075(3)	0.005(0)
118	(80, 32, 6)	26.161426(8)	3.316(7)	2.115(5)	0.961(3)	0.028(6)	0.068(5)	0.007(1)
119	(81, 32, 6)	26.315442(5)	3.323(7)	2.115(6)	0.962(4)	0.036(8)	0.069(8)	0.003(1)
120	(82, 32, 6)	26.468996(0)	3.330(8)	2.115(7)	0.962(0)	0.037(4)	0.070(2)	0.004(0)
121	(83, 32, 6)	26.622118(4)	3.337(9)	2.115(4)	0.961(4)	0.038(1)	0.067(6)	0.002(8)
122	(84, 32, 6)	26.774879(2)	3.344(9)	2.115(5)	0.962(0)	0.039(8)	0.068(5)	0.003(7)
123	(83, 34, 6)	26.927194(9)	3.367(2)	2.149(3)	0.962(5)	0.036(7)	0.085(6)	0.004(3)
124	(84, 34, 6)	27.079019(5)	3.374(1)	2.149(1)	0.962(7)	0.034(4)	0.086(7)	0.009(6)
125	(84, 34, 7)	27.230457(6)	3.388(4)	2.185(0)	1.034(0)	0.035(9)	0.085(2)	0.062(7)
126	(84, 35, 7)	27.381438(1)	3.402(7)	2.200(9)	1.034(1)	0.036(9)	0.089(2)	0.067(6)
127	(85, 35, 7)	27.532034(0)	3.409(4)	2.201(4)	1.034(0)	0.040(1)	0.091(0)	0.042(8)
128	(85, 35, 8)	27.682123(2)	3.423(5)	2.235(8)	1.092(2)	0.040(7)	0.083(2)	0.036(8)
129	(85, 36, 8)	27.831888(6)	3.437(9)	2.250(2)	1.091(9)	0.032(8)	0.081(5)	0.034(1)
130	(86, 36, 8)	27.981234(3)	3.444(5)	2.250(1)	1.091(7)	0.035(2)	0.083(2)	0.048(8)
131	(87, 36, 8)	28.130244(0)	3.451(3)	2.249(8)	1.090(9)	0.034(2)	0.078(5)	0.030(5)
132	(87, 37, 8)	28.278862(5)	3.465(1)	2.264(9)	1.090(5)	0.034(4)	0.081(8)	0.014(0)
133	(88, 37, 8)	28.427061(5)	3.471(8)	2.264(2)	1.091(2)	0.035(5)	0.085(7)	0.013(4)
134	(88, 37, 9)	28.574953(4)	3.485(5)	2.297(0)	1.144(0)	0.031(2)	0.071(5)	0.054(1)
135	(88, 38, 9)	28.722421(1)	3.499(2)	2.311(0)	1.143(6)	0.030(2)	0.073(9)	0.048(8)

Continuation of Table 1

N	Config.	E/N	r_1	r_2	r_3	σ_1	σ_2	σ_3
136	(89, 38, 9)	28.869526(8)	3.505(4)	2.311(2)	1.144(0)	0.031(5)	0.078(7)	0.043(7)
137	(90, 38, 9)	29.016328(0)	3.511(9)	2.311(0)	1.144(0)	0.033(4)	0.078(9)	0.040(2)
138	(90, 39, 9)	29.162701(3)	3.525(4)	2.325(1)	1.143(3)	0.029(9)	0.080(5)	0.037(0)
139	(91, 39, 9)	29.308773(6)	3.531(6)	2.325(1)	1.143(0)	0.034(2)	0.085(7)	0.034(9)
140	(91, 40, 9)	29.454518(1)	3.544(9)	2.339(1)	1.142(9)	0.029(5)	0.084(2)	0.042(4)
141	(92, 40, 9)	29.599899(6)	3.551(4)	2.338(7)	1.141(7)	0.033(5)	0.075(1)	0.038(4)
142	(92, 40, 10)	29.744962(8)	3.564(4)	2.368(9)	1.193(0)	0.034(1)	0.070(0)	0.045(4)
143	(93, 40, 10)	29.889733(5)	3.570(7)	2.368(9)	1.193(2)	0.031(4)	0.071(4)	0.032(2)
144	(94, 40, 10)	30.034090(4)	3.576(9)	2.368(8)	1.193(1)	0.033(1)	0.070(7)	0.055(2)
145	(94, 41, 10)	30.178106(2)	3.589(8)	2.382(5)	1.192(0)	0.035(8)	0.071(2)	0.034(8)
147	(95, 42, 10)	30.465219(1)	3.608(7)	2.395(7)	1.192(3)	0.029(9)	0.079(4)	0.039(4)
148	(96, 42, 10)	30.608238(9)	3.614(8)	2.395(5)	1.192(3)	0.030(6)	0.078(8)	0.036(7)
149	(96, 43, 10)	30.750998(2)	3.627(3)	2.409(0)	1.192(6)	0.032(3)	0.085(3)	0.037(6)
150	(96, 42, 12)	30.893383(1)	3.639(5)	2.454(1)	1.281(6)	0.034(8)	0.079(5)	0.010(3)
151	(96, 43, 12)	31.035390(0)	3.652(4)	2.465(9)	1.281(4)	0.027(1)	0.068(5)	0.014(6)
152	(96, 44, 12)	31.177075(2)	3.664(9)	2.478(3)	1.281(1)	0.031(1)	0.067(4)	0.016(5)
153	(97, 44, 12)	31.318527(6)	3.670(8)	2.478(1)	1.281(1)	0.028(2)	0.067(3)	0.012(9)
154	(98, 44, 12)	31.459632(1)	3.676(9)	2.477(7)	1.281(0)	0.026(3)	0.062(5)	0.014(4)

Continuation of Table 1

N	Config.	E/N	r_1	r_2	r_3	r_4
155	(98, 44, 12, 1)	31.600488(0)	3.688(7)	2.504(2)	1.384(6)	0.002(2)
156	(98, 45, 12, 1)	31.741100(1)	3.700(6)	2.516(9)	1.383(8)	0.012(7)
157	(100, 44, 12, 1)	31.881320(7)	3.700(4)	2.503(8)	1.383(9)	0.004(3)
158	(100, 45, 12, 1)	32.021293(6)	3.712(2)	2.516(6)	1.383(4)	0.004(3)
159	(101, 45, 12, 1)	32.161014(1)	3.718(0)	2.516(4)	1.383(7)	0.005(3)
160	(102, 45, 12, 1)	32.300404(8)	3.723(8)	2.516(1)	1.383(3)	0.007(3)
N		σ_1	σ_2	σ_3	σ_4	
155		0.030(1)	0.079(9)	0.009(0)	-	
156		0.033(3)	0.087(1)	0.006(2)	-	
157		0.034(0)	0.076(2)	0.006(5)	-	
158		0.032(7)	0.085(2)	0.006(3)	-	
159		0.031(0)	0.088(1)	0.005(9)	-	
160		0.034(1)	0.082(2)	0.005(2)	-	